Errandonea, D.; Manjón Herrera, FJ.; Muñoz, A.; Rodríguez-Hernández, P.; Panchal, V.; Achary, SN.; Tyagi, AK. (2013). High-pressure polymorphs of TbVO4: A Raman and ab initio study. Journal of Alloys and Compounds. 577:327-335. doi:10.1016/j.jallcom.2013.06.008.

High-pressure polymorphs of $TbVO_4$: A Raman and *ab initio* study

D. Errandonea[1,†], F.J. Manjón[2], A. Muñoz[3], P. Rodríguez-Hernández[3], V. Panchal[1,4], S.N. Achary[5], and A.K. Tyagi[5]

[1] Departamento de Física Aplicada-ICMUV, Universidad de Valencia, MALTA Consolider Team, Edificio de Investigación, C/Dr. Moliner 50, 46100 Burjassot (Valencia), Spain

[2] Instituto de Diseño para la Fabricación y Producción Automatizada, MALTA Consolider Team, Universidad Politécnica de Valencia, Camino de Vera s/n, 46022 Valencia, Spain

[3] Departamento de Física Fundamental II, Instituto de Materiales y Nanotecnología, MALTA Consolider Team, Universidad de La Laguna, La Laguna 38205, Tenerife, Spain

[4] Royal College of Arts, Science and Commerce, Mira Road, Mumbai 401107, India

[5] Chemistry Division, Bhabha Atomic Research Centre, Trombay, Mumbai 400085, India

Abstract: Raman measurements on $TbVO_4$ show the occurrence of three pressure-induced phase transitions. The first one, an irreversible transition from the zircon to the scheelite structure, occurs beyond 6.7 GPa. Additionally, two reversible phase transitions occur at 26.7 GPa and 34.4 GPa. The last transition was never reported before. The experimental findings are well supported by structural and lattice-dynamics calculations that have helped us to identify the post-scheelite phase as a monoclinic fergusonite structure. According to calculations, the third phase transition involves a symmetry increase. An orthorhombic structure is proposed for the high-pressure phase found above 34.4 GPa. The results have been compared with previous studies in $TbVO_4$ and discussed in comparison with related vanadates. The calculated equation of state is reported for the different polymorphs of $TbVO_4$. An increase of compressibility is caused by the third phase transition, being associated to the delocalization of Tb *f*-electrons. No evidence of metallization is experimentally detected nor predicted by theory.

Keywords: Raman spectroscopy, ab initio calculations, pressure-driven transitions, equation of state, zircon oxides.

[†] Corresponding author; email: daniel.errandonea@uv.es

I. Introduction

Orthovanadates are technologically important materials and find applications in cathodoluminescence, lithium ion batteries and as thermophosphors, scintillators, or photocatalysis materials [1, 2]. They are also used as laser-host materials when doped with trivalent impurities due to their high-optical conversion efficiency, high birefringence, and good thermal conductivity [3]. Rare-earth orthovanadates also show interesting structural and magnetic transformations at low temperatures [4] and a few are incomparable undergoing Jahn–Teller distortion [5, 6].

AVO_4 (with A = Y, Sc, Bi, or a trivalent lanthanide) oxides mostly crystallize in the tetragonal zircon-type structure (space group: $I4_1/amd$, Z = 4) [7] with few exceptions like $LaVO_4$, which adopts the monoclinic monazite structure at ambient conditions [8]. $TbVO_4$ has the zircon structure, which can be viewed as alternating edge-sharing AO_8 dodecahedra and VO_4 tetrahedra forming chains parallel to the *c*-axis. Upon compression most zircon-structured orthovanadates undergo zircon to scheelite (space group: $I4_1/a$, Z = 4) phase transitions [9 - 16]. However, orthovanadates like $CeVO_4$ experience zircon to monazite (space group: $P2_1/n$, Z = 4) phase transitions [14, 16]. Similarly, according to x-ray diffraction (XRD) studies, phosphates, arsenates, and chromates undergo either zircon to scheelite or zircon to monazite transitions [17 - 20]. In many compounds, such transitions have been discovered by means of high-pressure (HP) Raman measurements. In the case of $TbPO_4$, Raman experiments and lattice-dynamic calculations supported by XRD indicate a zircon to monazite phase transition at 9.5 GPa [21, 22]. On the contrary, $TbVO_4$ is observed to undergo a zircon to scheelite phase transition at 6.5 GPa [14, 23]. On top of that, a second transition from scheelite to monoclinic fergusonite (space group: $I2/a$, Z = 4) has been recently reported [14]. All these facts show that zircon-type ABO_4

oxides may follow different HP structural sequences depending upon the selection of A and B cations and the A/B radius ratio [22] and that further studies are requested to better understand the HP behavior of zircon-type oxides. Another reason to explore the HP polymorphism of $TbVO_4$ is that the scheelite-fergusonite transformation is typical of scheelite-type oxides [24]. Because of this fact, it has been proposed that the zircon-scheelite-fergusonite (Z-S-F) transitions could be a common behavior followed upon compression by many ABO_4 oxides; e.g. YVO_4 and $ThGeO_4$ [12, 25]. Additionally, the Z-S-F structural sequence is interesting for basic research because of the group-subgroup relationship ($I4_1/amd \rightarrow I4_1/a \rightarrow I2/a$) involved.

In the present investigation, we report Raman scattering measurements and *ab initio* calculations in $TbVO_4$ up to 36.6 GPa. The zircon-scheelite-fergusonite structural sequence is confirmed and a third transition to a higher symmetry structure found at 34.4 GPa. We report an analysis of the Raman-active modes of the different structures which can provide clues to understand the pressure-induced phase transition mechanisms in zircon-structured orthovanadates, orthophosphates, and orthochromates. The equations of state and electronic properties of the different phases are also discussed.

II. Experimental details

Polycrystalline $TbVO_4$ used in the experiments was prepared by solid-state reaction of appropriate amounts of predried Tb_2O_3 (Indian Rare Earth Ltd. 99%) and V_2O_5 (Alfa-Aesar 99%). Details of sample preparation can be found in Ref. [14]. The sample obtained was characterized by powder x-ray diffraction data recorded on a Panalytical X-pertPro diffractometer using Cu K_α radiation. A single phase with the zircon-type structure was confirmed with unit-cell parameters a = 7.166(7) Å and c = 6.317(6) Å.

Two independent Raman experiments were carried out, one up to 26.3 GPa and the second one up to 36.6 GPa. In each experiment, a small pellet (40 μm in size, 20 μm thick) obtained from the $TbVO_4$ sample was used. The pellet was loaded, along with 1-μm-diameter ruby balls, inside a 120-μm-diameter hole drilled on a 200-μm-thick Inconel gasket pre-indented to 40 μm and inserted between the diamonds of a 350-μm-culet diamond-anvil cell (DAC). A 16:3:1 methanol-ethanol-water mixture was used as pressure-transmitting medium [26, 27]. The pressure was determined by monitoring the shift in ruby fluorescence lines [28]. HP Raman measurements were performed in the backscattering geometry using 632.8 nm HeNe laser and a Horiba Jobin Yvon LabRAM HR UV microspectrometer in combination with a thermoelectric-cooled multichannel CCD detector with spectral resolution below 2 cm^{-1}.

III. Theoretical method and computational details

Ab initio simulations have been performed within the density-functional theory (DFT) framework as implemented in the Vienna *ab initio* simulation package (VASP) (see Refs. 29 and 30 and references therein). The program performs *ab initio* structural calculations with the plane-wave pseudo-potential method. The set of plane waves employed extended up to a kinetic energy cutoff of 520 eV. Such a large cutoff was required to achieve highly converged results within the projector-augmented-wave (PAW) scheme [30, 31]. The PAW method takes into account the full nodal character of the all-electron charge density distribution in the core region. It is known that standard DFT does not work properly for strongly localized *f* electrons. To deal with this problem, we adopted the standard procedure to treat the *f* electrons using a PAW pseudopotential [32, 33]. For the Tb atom, all the *f* electrons except one are frozen in the core during the pseudopotential generation. The exchange-correlation energy was taken in the generalized gradient approximation (GGA) with the Perdew-Burke-Ernzerhof (PBE) prescription [34]. It is

well known that the GGA approach underestimates the cohesion energy [35] (producing an overestimation of the equilibrium volume). We used dense special point grids appropriate to each structure considered to sample the Brillouin zone (BZ), thus ensuring a high convergence of 1–2 meV per formula unit in the total energy of each structure as well as an accurate calculation of the forces on the atoms. At each selected volume, the structures were fully relaxed to their equilibrium configurations through the calculation of the forces on atoms and the stress tensor [35]. In the relaxed equilibrium configuration, the forces were smaller than 0.005 eV/Å, and the deviation of the stress tensor from a diagonal hydrostatic form was less than 0.1 GPa.

Lattice-dynamic calculations of phonon modes were performed in zircon, scheelite, fergusonite, and the rest of relevant structures at the zone center (Γ point) of the BZ. We used a direct force-constant approach (or supercell method) [36]. These calculations provide information about the symmetry of the modes and their polarization vectors, and allowed us to identify the irreducible representations and the character of the phonon modes at the Γ point.

IV. Results

A. Raman experiments

$TbVO_4$ crystallizes in the zircon structure (*$I4_1/amd$*, point group *D_{4h}*) with two formula units per primitive cell. The group theoretical analysis predicts twelve Raman-active modes at the center of the BZ with symmetries $\Gamma = 2A_{1g} + 4B_{1g} + B_{2g} + 5E_g$ [37]. These modes can be further classified into internal (ν_1-ν_4) and external (translational, T, and rotational, R) modes of VO_4 units as follows,

$$\Gamma = A_{1g}(\nu_1, \nu_2) + B_{1g}(2T, \nu_3, \nu_4) + B_{2g}(\nu_2) + E_g(2T, R, \nu_3, \nu_4). \quad (1)$$

Figure 1(a) shows representative Raman spectra of zircon-type $TbVO_4$ at various pressures up to 6.7 GPa. These spectra were collected in the experimental run performed up to

26.3 GPa. We have observed nine out of twelve Raman peaks at ambient conditions. All the Raman modes observed can be divided in two broad frequency regions, the low-frequency region from 100-500 cm^{-1} and the high frequency region from 750-950 cm^{-1} with a frequency gap between 500 and 750 cm^{-1}. The symmetry assignment for the Raman modes has been performed in accordance with our calculations and by comparison with previous results in $TbVO_4$, altogether summarized in **Table I**. Our Raman frequencies at ambient pressure agree well with the literature [23, 38], being differences in frequencies always within 1%.

As can be seen from **Fig. 1(a)**, the Raman spectrum of zircon-type $TbVO_4$ is dominated by the intense symmetric-stretching internal mode $\nu_1(A_{1g})$, located at 885 cm^{-1} at ambient pressure, and two asymmetric-stretching modes $\nu_3(E_g)$ and $\nu_3(B_{1g})$ at 826 and 809 cm^{-1}, respectively. Out of the four bending modes of the VO_4 unit we could observe only three modes: $\nu_4(B_{1g})$ at 483 cm^{-1}, $\nu_4(A_{1g})$ at 381 cm^{-1}, and $\nu_2(B_{2g})$ at 260 cm^{-1}. Neither the asymmetric-bending mode $\nu_4(E_g)$ nor the two external translational $T(E_g)$ and $T(B_{1g})$ modes could be detected in $TbVO_4$. These modes, and especially the two translational modes, are also absent in most of the Raman scattering measurements performed in other orthovanadates probably due to their weak Raman scattering cross-section [37, 38]. Curiously, they have been found recently in polarized Raman measurements in YVO_4 at ambient pressure [39].

Figure 1(b) shows the pressure dependence of Raman modes in the zircon phase. The symmetry assignment for the Raman modes along with their experimental and calculated frequencies, pressure coefficients, and mode Grüneisen parameters (γ) are shown in **Table I**. We have found good agreement between experimental and calculated frequencies and pressure coefficients for the Raman modes. The Grüneisen parameters of the different modes in the zircon phase have been obtained by using the bulk modulus B_0 = 122 GPa reported earlier by XRD

measurements on $TbVO_4$ [14]. The pressure coefficients here obtained for the nine reported phonons compare quite well with those reported by Duclos *et al*. [23].

All the Raman modes of the zircon phase exhibit positive pressure coefficients except for the external $T(E_g)$ mode at 154 cm^{-1} and the internal $\nu_2(B_{2g})$ mode at 260 cm^{-1} at ambient pressure. Some modes merge upon compression due to their different pressure evolution (see **Fig. 1b**). A similar behavior has been observed in other orthovanadates like $ScVO_4$ [9], YVO_4 [12], $LuVO_4$ [13], $CeVO_4$ [16], and $YbVO_4$ [15]. The softening of the two modes might be associated with a mechanical instability of the zircon phase, leading to the zircon to scheelite phase transition. The pressure coefficient of the $\nu_2(B_{2g})$ bending soft-mode is found to be -1.2 cm^{-1}/GPa which is in good agreement with -1.3 cm^{-1}/GPa reported in an earlier Raman investigation [23]. Similar values of the order of -1.2 to -1.4 cm^{-1}/GPa have been found among other orthovanadates [9, 12, 13, 15, 16]. Correspondingly, the pressure coefficient of the $T(E_g)$ soft-mode at 154 cm^{-1} is -0.4 cm^{-1}/GPa, being in agreement with the earlier reported value, -0.42 cm^{-1}/GPa [23]. For this mode, values of the pressure coefficients between -0.22 and 1.0 cm^{-1}/GPa have been published in other orthovanadates [9, 12, 13, 15, 16]. A completely different behavior occurs for the rotational $R(E_g)$ mode of orthovanadates, which shows the largest positive pressure coefficient among the external modes of the VO_4 tetrahedra; about 4-6 cm^{-1}/GPa [9, 12, 13, 14, 16]. In general, very similar pressure coefficients for the different Raman modes are found in all orthovanadates.

Important changes appear in Raman spectra above 6.7 GPa, as can be seen by comparing **Fig. 1(a)** and **Fig. 2(a)** which show spectra collected in the same experimental run. **Figure 2(a)** shows a selection of Raman spectra measured from 8.3 up to 26.3 GPa. At 8.3 GPa, the appearance of extra Raman peaks and other subtle changes suggest a phase transition. In fact, the

changes observed in the Raman spectra are similar to those previously reported by Duclos *et al*. [23] and are consistent with the occurrence of the zircon to scheelite phase transition. The transition pressure is also in agreement with that obtained from XRD experiments [14].

Group theoretical calculations for scheelite-type $TbVO_4$ (space group: $I4_1/a$, point group C_{4h}^6) predict thirteen first-order Raman modes at the BZ centre with following symmetries $\Gamma = 3A_g + 5\ B_g + 5\ E_g$ [40, 41]. These modes can be further classified either as internal (ν_1 to ν_4) or external (T and R) modes of the VO_4 units,

$$\Gamma = A_g\ (R,\nu_1,\nu_2) + B_g\ (2T,\ \nu_2,\nu_3,\nu_4) + E_g\ (2T,R,\nu_3,\nu_4) \qquad (2)$$

The symmetry assignment for the Raman modes of $TbVO_4$ in the scheelite phase is summarized in **Table II** and has been performed in accordance with our lattice-dynamics calculations and by comparison with previous results in other vanadates. Out of thirteen Raman-active modes expected in the scheelite phase, we observed only twelve modes at 8.3 GPa [see **Fig. 2(a)**]. Beyond this pressure we were able to detect the only missing mode; i.e., the low frequency translational $T(E_g)$ mode located at 119 cm^{-1} at 9.6 GPa. This mode was previously not reported in the previous experiment of Duclos *et al*. [23] because of the frequency cut-off of the used experimental set-up.

As regards the Raman modes in scheelite-type $TbVO_4$, the Raman spectrum is dominated by the highest frequency mode at 861 cm^{-1}, which is assigned to the symmetric stretching mode $\nu_1(A_g)$. Its frequency is observed to be the highest among the known scheelite-type ortovanadates [9, 12, 13, 15, 23]. Two asymmetric-stretching modes of the scheelite phase of $TbVO_4$ are observed around 831 and 779 cm^{-1} and assigned to $\nu_3(B_g)$ and $\nu_3(E_g)$ modes, respectively. Similarly, four bending modes observed experimentally at 459, 434, 389, and 246 cm^{-1} have been assigned to the $\nu_4(E_g)$, $\nu_4(B_g)$, $\nu_2(B_g)$, and $\nu_2(A_g)$ modes, respectively. In addition, we have

found the six external modes predicted for the scheelite phase. All the experimentally observed Raman modes show positive pressure coefficient except the translational T(B_g) mode located at 140 cm^{-1}. For this mode, we have obtained a slightly negative pressure coefficient, while previously a slightly positive value close to zero was reported [23]. Our calculations confirm the softening of this T(B_g) mode which is typical of orthotungstates and orthomolybdates that undergo the scheelite-to-fergusonite transition [42].

In **Fig. 3(a)** we summarized the data obtained from the second experimental run. In agreement with the first run, the transition to the scheelite phase is detected at 8.8 GPa. We observed this phase (denoted as phase II) to remain stable up to 25.8 GPa. Upon further pressure increase, at 26.7 GPa changes occur in the Raman spectrum indicating the occurrence of a second transition to phase III. This transition was not detected in the first experiment because it takes place at a pressure 0.4 GPa higher than the maximum pressure reached on it. Phase III is found to be stable up to 31.4 GPa. In a subsequent compression step, at 34.4 GPa an additional phase transition to phase IV is found, which was not detected by XRD [14]. Phase IV is observed up to 36.6 GPa with no evidence of chemical decomposition or amorphization of $TbVO_4$. The differences regarding phase IV could be due to the presence of deviatoric stresses in our sample induced by the used pressure medium. These stresses were smaller in the diffraction experiments because neon was the pressure medium [14]. Deviatoric stresses have been shown to influence the HP structural sequence in related oxides and to reduce transition pressures [43, 44]. Upon decompression phases III and II (scheelite) are recovered at 31.5 and 25.4 GPa, respectively. After fully releasing the pressure the scheelite phase is recovered; see spectrum at 1.6 GPa in **Fig. 3(a)**. This indicates that the zircon to scheelite transition is irreversible, irrespective of the experiment hydrostaticity. The same fact was observed when releasing pressure from 26.3 GPa

in the other run. Frequencies of the Raman modes were obtained for the scheelite phase upon pressure release at 1.6 GPa from the spectrum reported in **Fig. 3(a)**. **Table III** summarizes the eighteen Raman-active modes detected in phase III and their pressure coefficients. The possible crystal structures and phonons of phases III and IV will be discussed in next section. As we will show, there is enough evidence to assign phase III to the fergusonite structure.

B. Structural calculations

Figure 4 shows the energy as a function of volume curves for all the calculated structures, a transition occurs when two phases have the same enthalpy at the transition pressure. The zero-point energy and the temperature effects were included using the quasi-harmonic approximation. It allows us to obtain the free energy as a function of pressure, which is shown in the inset of the figure for the relevant structures. The rest of the calculated structures are very high in enthalpy and are not candidates to HP phases. The considered structures include not only zircon, scheelite, and fergusonite structures (*C2/c* standard setting and *I2/a* non-standard setting), but also orthorhombic structures previously proposed for related compounds (Cmca and $SrUO_4$-type) [45], and monoclinic monazite-type ($P2_1/n$) [46] and BaWO4-II-type ($P2_1/n$) [42] structures. Our theoretical study indicates that the zircon-type is the structure of $TbVO_4$ with the lowest free energy at ambient pressure. The calculated structural parameters at ambient pressure and selected pressures for the different phases are given in **Table IV**. A fit with a Birch-Murnaghan fourth-order equation of state (EOS) [47] gives for the zircon structure values in good agreement with experimental results: V_0 = 332.45 Å^3, B_0 = 124.2 GPa, B_0'= 5.18, and B_0'' = -0.0004 GPa^{-1}. The equilibrium volume V_0 is overestimated by 2.4 %, as usual with the GGA approximation [48, 49]. The bulk modulus B_0 is overestimated by a similar proportion with respect to the experimental value.

Upon compression our calculations predict the occurrence of several phase transitions: Zircon-to-scheelite at 5.4 GPa, scheelite-to-fergusonite at 26 GPa, and fergusonite-to-Cmca at 32.8 GPa. The first transition is in agreement with present and previous experiments. It is a first-order transition that involves a large volume collapse ($\Delta V/V$ = 11.02%). The tetragonal scheelite-type structure ($I4_1/a$) also consists of TbO_8 bisdisphenoids and VO_4 tetrahedra [45]. The structural relation between both zircon and scheelite structures has been nicely described by Nyman *et al.* [50]. The scheelite-to-fergusonite transition is more subtle than the zircon-to-scheelite phase transition. Structural optimization indicates that the fergusonite structure, which is a slight monoclinic distortion of the scheelite structure [45], reduces to the scheelite structure below 24 GPa. This can be seen in **Fig. 5** where we represent the monoclinic β angle of the fergusonite phase vs. pressure. Calculations were carried out using the standard setting, but in order to better illustrate the relationship between fergusonite and scheelite structures, we used in **Fig. 5** the β angle of the non-standard *I2/a* setting of the fergusonite structure [45] (in this description for β = 90º and $a = c$ the fergusonite structure reduces into scheelite structure). According to our calculations, the fergusonite phase only emerges as the thermodynamically stable phase above a compression threshold of about 26 GPa. However, the energy and the enthalpy differences in favor of fergusonite are so small that cannot be easily distinguished in **Fig. 4**. The transition pressure for the second transition is consistent with the transition pressure of the second transition detected in our Raman experiments. The scheelite-to-fergusonite phase transition is a continuous or quasi-continuous transition with no volume collapse. This phase transition is of second-order nature according to Landau's theory and has been previously detected in many orthotungstates and orthomolybdates, and in some orthovanadates, like YVO_4 and $ScVO_4$ at 20 and 18.2 GPa, respectively [9, 12, 42, 51, 52].

In the course of structural optimization under further compression, we have arrived to a structure that becomes thermodynamically more stable than zircon, scheelite, and fergusonite phases at 32.8 GPa and higher pressures in $TbVO_4$. This structure has an orthorhombic symmetry, with space group Cmca and double number of atoms in the unit cell (Z = 8) than the other structures. In this structure, the Tb and V cations are surrounded by ten and six O atoms, respectively. This third transition occurs at a pressure similar to the observed transition pressure to phase IV. The transition involves a large volume collapse of $\Delta V/V$ = 11.8 %. As we will discuss latter, the Cmca structure supposes an increase of the number of Raman-active modes. We would like to add here, that we found another orthorhombic structure, $SrUO_4$-type (space group: *Pbcm*) to be thermodynamically competitive regarding stability with the Cmca structure (see **Fig. 4**). However, we found the $SrUO_4$-type structure to have six phonons with negative frequencies (one Raman, one silent, and four infrared modes), being therefore mechanically unstable, which leaded to the exclusion of this structure as a candidate HP phase of $TbVO_4$.

The equation of state for each of the HP phases has been calculated. For the tetragonal scheelite phase we obtained V_0 = 294.69 $Å^3$, B_0 = 140.8 GPa, B_0'= 4.64, and B_0'' = -0.0769 GPa^{-1}. For the monoclinic fergusonite phase we obtained V_0 = 294.33 $Å^3$, B_0 = 142.7 GPa, B_0'= 5.87, and B_0'' = -0.3106 GPa^{-1}. For the orthorhombic phase we obtained V_0 = 524.66 $Å^3$, B_0 = 134.3 GPa, B_0'= 3.38, and B_0'' = -0.0022 GPa^{-1}. None of the structures shows anomalous positive values for the second pressure derivative of the bulk modulus. Therefore, the rate at which the four phases become stiffer decreases with increasing pressure. Note that the scheelite phase is less compressible than the zircon phase. This fact has been observed in other vanadates [14] and in phosphates [17] and it is related with the increase of the packing efficiency in the scheelite structure. The calculated bulk modulus at ambient pressure for scheelite $TbVO_4$ is

approximately 12% smaller than the measured one [14]. Changes in compression are less important at the scheelite-to-fergusonite transition as observed in molybdates [52] and tungstates [45]. For the orthorhombic structure an interesting fact is predicted by calculations: a reduction of 7% of the bulk modulus in the HP phase. Similar phenomena are rarely observed to occur under compression, being a manifestation of a localized-to-delocalized electronic transition [53]. In the present case, our calculations show that the unexpected reduction of the bulk modulus is related to the well-known *f*-electron delocalization induced by pressure in lanthanides [54 – 56].

C. Lattice-dynamics calculations

In order to correlate changes observed in Raman spectra with phase transitions predicted by theory, we conducted lattice-dynamics calculations using the method described in Sec. III. These calculations were performed after structural optimization. From them, we have obtained the frequencies and pressure dependence of all normal modes in the zircon, scheelite, fergusonite, and Cmca phases. For the sake of briefness we will report here only the calculated Raman frequencies, which are given in **Tables I, II, III,** and **V** together with the experimental ones. **Figs. 1(b)** and **2(b)** show the pressure dependence of the calculated Raman frequencies for both zircon and scheelite phases. There is very good overall agreement between experiments and theoretical results of mode frequencies at the equilibrium volume for each phase and of their pressure dependence (see **Tables I** and **II**). For the zircon structure we have also calculated the phonon dispersion and density of states (DOS), with the local contribution of each atom, which are shown in **Fig. 6**. Clearly the phonons related with the vibration of Tb atoms are below 200 cm^{-1}, and the vibrations of the V and O atoms are the responsible of the rest of phonons.

In addition to Raman modes, there is a notable feature that deserves to be remarked. It is the behavior of the B_{1u} silent mode (95.6 cm^{-1} at ambient pressure) of the zircon phase. This

mode has a strong non-linear dependence. It can be assigned to rotations of rigid $(VO_4)^{3-}$ units and transforms to an also silent B_u symmetry mode in the scheelite phase. We found it to exhibit a soft-mode behavior with pressure. At 7.2 GPa, its frequency becomes negative. A plot of calculated frequencies of this soft mode with pressure across the phase transition is given in **Fig. 7**. We believe the presence of this mode and the two Raman-active soft modes are related to mechanical instabilities of the zircon structure [57].

Regarding the scheelite structure, the agreement of our calculations with the experiments is also excellent, being the pressure coefficients in general slightly underestimated. Calculations as experiments found the existence of a soft mode, very typical of scheelite-structure compounds [40] and usually related to the occurrence of the ferroelastic scheelite-fergusonite phase transition. In particular, the atomic movements associated to the B_g soft mode (140 cm^{-1}) are consistent with the displacement of the VO_4 at the scheelite-to-fergusonite transition [58]. Calculations, as experiments, show a merging of some Raman modes under compression due to their different evolution [see **Fig. 2(b**)].

As described before, our calculations found that the second HP phase has a monoclinic fergusonite structure. Group theoretical calculations for the fergusonite phase (space group *C2/c* or *I2/a*, point group C^6_{2h}) predict eighteen first-order Raman modes at the Brillouin-zone center with symmetries $\Gamma = 8A_g + 10B_g$. The correlation between the scheelite and fergusonite Raman modes is as follows: every A_g and B_g scheelite mode converts into an A_g mode of monoclinic symmetry while every doubly degenerate E_g mode converts into two B_g modes. The calculated phonons qualitatively reproduce the measured Raman spectra for phase III. Ticks at the bottom of Raman spectrum at 31.4 GPa in **Fig. 3(a)** give the position of the calculated modes. The agreement for pressure coefficients is not as good as for the frequencies (see **Table III**), giving

the calculations larger pressure coefficients than experiments. According to theory, there are four high-frequency internal modes in the fergusonite phase [40, 41] as observed in the experiments of $TbVO_4$ for phase III. Besides, calculations and experiments show the appearance of three modes in the frequency region corresponding to the phonon gap of scheelite (consequently the phonon gap is reduced). According to calculations, the fergusonite phase has one soft-mode, the lowest frequency A_g mode (see **Table III**), which has a pressure coefficient of -0.58 cm^{-1}. However, experiments found this mode to have a small positive pressure coefficient of 0.4 cm^{-1}. Possible causes, for this discrepancy could be the fact that calculations are performed neglecting anharmonic effects. Based upon the above describe similarities between the results extracted from Raman measurements and lattice-dynamics calculations, in the structural calculations, and in the detection of the fergusonite phase in x-ray diffraction experiments [14], we conclude there is enough evidence to confirm that $TbVO_4$ follows the zircon-scheelite-fergusonite structural sequence as its isomorphic compounds with small trivalent cations [9, 11, 12]; e.g. Eu and Lu.

Finally, we would like to comment on the calculated Raman modes of the orthorhombic Cmca structure (point group symmetry D_{2h}). Group theory predicts for it thirty-six first-order Raman modes: $\Gamma = 9B_{1g} + 7B_{2g} + 11B_{3g} + 9A_g$. The calculated modes and pressure coefficients are summarized in **Table V**. The duplication of the number of modes (and the enhancement of deviatoric stresses due to the used pressure medium) can be the cause of the appearance of broad bands in the Raman spectrum of phase IV. According to calculations, the Cmca phase has one soft mode (720.3 cm^{-1}) and the hardest mode is the highest frequency B_{2g} mode (748.2 cm^{-1}). In comparison with experiments, there is a noticeable difference. All calculated modes have frequencies smaller than 807 cm^{-1}. A possible explanation to the presence of these modes might be the coexistence of phases III and IV at pressure higher than the transition onset.

Unfortunately, in the experiments there are several modes detected between 800 and 1000 cm^{-1}. Therefore, no definitive conclusions can be extracted on the crystal structure of phase IV. Further theoretical and experimental studies are needed to clarify this point.

D. Comment on the electronic properties

Zircon-type $TbVO_4$ is expected to have a large electronic band-gap (3.7-3.8 eV) with the bottom of the valence band basically composed by V 3*d*–O 2*p* states and the top of valence band consisting of O 2*p* states [10]. For the scheelite phase, a band-gap collapse occurs in related vanadates [10]. The collapse is caused by a pressure-driven hybridization of electronic orbitals. As a consequence of it, a band-gap of 2.7 eV has been measured for the scheelite phase [23]. We confirm this fact by reflectance measurements performed in polycrystalline scheelite-type $TbVO_4$ quenched from 12 GPa using a large-volume press [59, 60]. Upon compression, due to the increase of electronic hybridization [10], the band-gap of scheelite-type $TbVO_4$ closes at a rate of –37 meV/GPa [23] as happens in other vanadates [10]. For the zircon and scheelite phases, we carried out band-structure calculations which are in good agreement with this picture. According with band-structure calculations the zircon and scheelite phases of $TbVO_4$ have a direct band gap. Since band structures are very similar to those of related vanadates [10], they will not be reported here for the sake of briefness. Extrapolating the behavior of the optical band gap of scheelite to extreme pressure, it has been argued that metallization can be induced by pressure in rare-earth vanadates [23]. If metallization would occur, $TbVO_4$ should become black and changes in sample reflectivity should be observed. None of these facts have been detected in our experiments for any of the three HP phases indicating that the band-gap overlap metallization does not occur in $TbVO_4$ up to 36.6 GPa. In order to confirm these conclusions, we performed band-structure calculations for the Cmca structure of $TbVO_4$ (the highest pressure phase) and

obtained that orthorhombic $TbVO_4$ is a direct band gap material with a band-gap of 1 eV. Therefore, both experiments and calculations do not point toward pressure-induced metallization in the pressure range covered by this study.

V. Conclusions

Our combined experimental and theoretical study of terbium orthovanadate up to 36.6 GPa confirms that the low-pressure zircon phase undergoes an irreversible zircon-to-scheelite phase transition above 6.7 GPa. In addition, a scheelite-to-fergusonite phase transition is detected at 26.7 GPa. Evidence of a third transition is found at 34.4 GPa. Calculations suggest that the phase observed beyond 34.4 GPa may have an orthorhombic structure. On release of pressure the last two transitions are reversible with little hystheresis. On the contrary, below 25.4 GPa the sample retains the metastable scheelite phase even at ambient pressure. The symmetries of the Raman modes in the zircon, scheelite, fergusonite, and orthorhombic phases of $TbVO_4$ have been assigned by use of lattice-dynamics calculations. In general, a good agreement is found between our experimental and theoretical data. The calculated equations of state for the different polymorphs are also reported. An anomalous increase of compressibility is predicted for the fergusonite-to-Cmca phase transition. It is apparently associated to the pressure-induced delocalization of *f*-electrons of Tb. Finally, no evidence of pressure-driven metallization of $TbVO_4$ is found in the pressure-range covered by the present studies.

Acknowledgements

Research supported by Spanish MINECO (Grants No: MAT2010-21270-C04-01/03/04), MALTA Consolider (CSD2007-00045), and Vicerrectorado de Investigación y Desarrollo of UPV (UPV2011-0966/0914). A. M. and P. R-H. acknowledge computing time provided by Red Española de Supercomputación and MALTA-Cluster.

References

[1] S. P. Shafi, M. W. Kotyk, L. M. D. Cranswick, V. K. Michaelis, S. Kroeker, and M. Bieringer, Inorganic Chemistry **48** (2009) 10553 and references therein.

[2] D. F. Mullica, E. L. Sappenifield, M. M. Abraham, B. C. Chakoumakos, and L. A. Boatner, Inorg. Chim. Acta **248** (1996) 85.

[3] C. Kränkel, D. Fagundes-Peters, S.T. Fredrich, J. Johannsen, M. Mond, G. Huber, M. Bernhagen and R. Uecker, Appl. Phys. B **79** (2004) 543.

[4] G.A. Ghering, K.A. Ghering, J. Mater. Sci. Lett. **2** (1975) 371.

[5] S.H. Smith, B.M. Wanklyn, J. Cryst. Growth **21** (1974) 23.

[6] R. J. Elliott, R. T. Harley, W. Hayes and S. Smith, Proc. R. Soc. Lond. A. **238** (1972) 217.

[7] T. Aldred, Acta Crystallogr. B **40** (1984) 569.

[8] J. Bashir, M. Nasir Khan, Materials Letters **60** (2006) 470.

[9] V. Panchal, F. J. Manjón, D. Errandonea, P. Rodríguez Hernández, J. López-Solano, A. Muñoz, S. N. Achary, and A. K. Tyagi, Phys. Rev. B **83** (2011) 064111.

[10] V. Panchal, D. Errandonea, A. Segura, P. Rodrıguez-Hernandez, A. Muñoz, S. Lopez-Moreno, and M. Bettinelli, J. Appl. Phys. **110** (2011) 043723.

[11] D. Errandonea, R. Lacomba-Perales, J. Ruiz-Fuertes, A. Segura, S. N. Achary, and A. K. Tyagi, Phys. Rev. **B 79** (2009) 184104.

[12] F. J. Manjón, P. Rodríguez-Hernández, A. Muñoz, A. H. Romero, D. Errandonea, K. Syassen, Phys. Rev. **B 81** (2010) 075202.

[13] R. Rao, A. B. Garg, T. Sakuntala, S. N. Achary, and A. K. Tyagi, J. Solid. State Chem. **182** (2009) 1879.

[14] D. Errandonea, R. S. Kumar, S. N. Achary, and A. K. Tyagi, Phys. Rev. B **84** (2011) 224121.

[15] A. B. Garg, R. Rao, T. Sakuntala, B. N. Wani, and V. Vijayakumar, J. Appl. Phys. **106** (2009) 063513.

[16] V. Panchal, S. Lopez-Moreno, D. Santamarıa-Perez, D. Errandonea, F. J. Manjon, P. Rodrıguez-Hernandez, A. Muñoz, S. N. Achary, and A. K. Tyagi, Phys. Rev. B **84** (2011) 024111.

[17] R. Lacomba-Perales, D. Errandonea, Y. Meng, and M. Bettinelli, Phys. Rev. B **81** (2010) 064113.

[18] F. X. Zhang, J. W. Wang, M. Lang, J. M. Zhang, and R. C. Ewing, Phys. Rev. B **80** (2009) 184114.

[19] F. X. Zhang, M. Lang, R. C. Ewing, J. Lian, Z. W. Wang, J. Hu, L. A. Boatner, J. Solid. State Chem. **181** (2008) 2633.

[20] D. Errandonea, R. Kumar, J. Lopez-Solano, P. Rodrıguez-Hernandez, A. Muñoz, M. G. Rabie, and R. Saez Puche, Phys. Rev. B **83** (2011) 134109.

[21] A. Tatsi, E. Stavrou, Y. C. Boulmetis, A. G. Kontos, Y. S. Raptis, and C. Raptis, J. Phys.: Condens. Matter **20** (2008) 425216.

[22] J. López-Solano, P. Rodríguez-Hernández, A. Muñoz, O. Gomis, D. Santamaría-Pérez, D. Errandonea, and F. J. Manjón, Phys. Rev. B **81** (2010) 144126.

[23] S. J. Duclos**,** A. Jayaraman**,** G. P. Espinosa**,** A. S. Cooper**,** and R.G. Maines, J. Phy. Chem. Sol. **50** (1989) 769.

[24] D. Errandonea and F.J. Manjón, Prog. Mat. Sci. **53** (2008) 711.

[25] D. Errandonea, R. S. Kumar, L. Gracia, A. Beltrán, S. N. Achary, and A. K. Tyagi, Phys, Rev. B **80** (2009) 094101.

[26] S. Klotz, L. Paumier, G. Le Marchand, and P. Munsch, J. Phys. D: Appl. Phys. **42** (2009) 075413.

[27] D. Errandonea, Y. Meng, M. Somayazulu, and D. Häusermann, Physica B **355** (2005)116.

[28] H. K. Mao, J. Xu, and P. M. Bell, J. Geophys. Res. **91**(1986) 4673.

[29] G. Kresse and J. Furthmuller,Phys. Rev. B **54** (1996) 11169.

[30] G. Kresse and D. Joubert,Phys. Rev. B **59** (1999) 1758.

[31] P. E. Blochl, Phys.Rev. B **50** (1994) 17953.

[32] J. Hafner, J. Comput. Chem. **29** (2008) 2044.

[33] C. J. Pickard, B. Winkler, R. K. Chen, M. C. Payne, M. H. Lee, J. S. Lin, J. A. White, V. Milman, and D. Vanderbilt, Phys. Rev. Lett. **85** (2000) 5122.

[34] J. P. Perdew, K. Burke, and M. Ernzerhof, Phys. Rev. Lett. **77** (1996) 3865.

[35] A. Mujica, A. Rubio, A. Muñoz, and R. J. Needs,Rev. Mod. Phys. **75** (2003) 863.

[36] K. Parlinski, computer code PHONON [http://wolf.ifj.edu.pl/phonon/].

[37] I. Guedes, Y. Hirano, M. Grimsditch, N. Wakabayashi, C. K. Loong, and L. A. Boatner, J. Appl. Phys. **90** (2001) 1843.

[38] C. C. Santos, E. N. Silva, A. P. Ayala, I. Guedes, P. S. Pizani, C. K. Loong, and L. A. Boatner, J. Appl. Phys. **101** (2007) 053511.

[39] A. Sanson, M. Giarola, B. Rossi, G. Mariotto, E. Cazzanelli, and A. Speghini, Phys. Rev. B **86** (2012) 214305.

[40] F. J. Manjón, D. Errandonea, N. Garro, J. Pellicer-Porres, P. Rodríguez-Hernández, S. Radescu, J. López-Solano, A. Mujica, and A. Muñoz, Phys. Rev. B **74** (2006) 144111.

[41] F.J. Manjon, D. Errandonea, N. Garro, J. Pellicer-Porres, P. Rodriguez-Hernandez, S. Radescu, J. Lopez-Solano, A. Mujica, and A. Muñoz, Phys. Rev. B **74** (2006) 144112.

[42] D. Errandonea and F. J. Manjon, Mat. Res. Bull. **44** (2009) 807.

[43] O. Gomis, J. A. Sans, R. Lacomba-Perales, D. Errandonea, Y. Meng, J. C. Chervin, and A. Polian, Phys. Rev. B **86** (2012) 054121.

[44] D. Santamarıa-Perez, L. Gracia, G. Garbarino, A. Beltran, R. Chulia-Jordan, O. Gomis, D. Errandonea, Ch. Ferrer-Roca, D. Martınez-Garcıa, and A. Segura,Phys. Rev. B **84** (2011) 054102.

[45] D. Errandonea, J. Pellicer-Porres, F. J. Manjón, A. Segura, Ch. Ferrer-Roca, R. S. Kumar, O. Tschauner, P. Rodríguez-Hernández, J. López-Solano, S. Radescu, A. Mujica, A. Muñoz, and G. Aquilanti, Phys. Rev. B **72** (2005) 174106.

[46] E. Bandiello, D. Errandonea, D. Martinez-Garcia, D. Santamaria-Perez, and F. J. Manjon, Phys. Rev. B **85** (2012) 024108.

[47] F. Birch, J. Geophys. Res. **83** (1978) 1257.

[48] R. Lacomba-Perales, D. Errandonea, D. Martinez-Garcia, P. Rodríguez-Hernández, S. Radescu, A. Mujica, A. Muñoz, J. C. Chervin, and A. Polian, Phys. Rev. B **79** (2009) 094105.

[49] D. Errandonea, D. Santamaría-Perez, A. Vegas, J. Nuss, M. Jansen, P. Rodríguez-Hernandez, and A. Muñoz, Phys. Rev. B **77** (2008) 094113.

[50] H. Nyman, B. G. Hyde, and S. Andersson, Acta Cryst. B **40** (1984) 441.

[51] D. Errandonea, EPL **77** (2007) 56001.

[52] D. Errandonea, R. S. Kumar, X. Ma, and C. Tu, J. Solid State Chem. **181** (2008) 355.

[53] F. Rivadulla, M. Bañobre-Lopez, C.X. Quintela, A. Piñeiro, V. Pardo, D. Baldomir, M.A. Lopez-Quintela, J. Rivas, C.A. Ramos, H. Salva, J.S. Zhou, and J.B. Goodenough, Nature Materials **8** (2009) 947.

[54] W. A. Grosshans and W. B. Holzapfel, Phys. Rev. B **45** (1992) 6603.

[55] D. Errandonea, R. Boehler, and M. Ross, Phys. Rev. Lett. **85** (2000) 3444.

[56] Y. Y. Boguslavskii, V. A. Goncharova, and G. G. Il'ina, Zh. Eksp. Teor. Fiz. **91** (1986) 1735.

[57] E. Stavrou, A. Tatsi, C. Raptis, I. Efthimiopoulos, K. Syassen, A. Muñoz, P. Rodrıguez-Hernandez, J. Lopez-Solano, and M. Hanfland, Phys. Rev. B **85** (2012) 024117.

[58] T. Da-Yong, X. Wan-Sheng, Z. Wei, C. Ming, X. Xiao-Lin, and S. Mao-Shuang, Chin. Phys. B **21** (2012) 086201.

[59] D. Errandonea, J. Appl. Phys. **108** (2010) 033517.

[60] D. Errandonea, A. Segura, D. Martínez-García, and V. Muñoz-San Jose, Phys. Rev. B **79** (2009) 125203.

Table I: Calculated and experimental frequencies at ambient conditions (ω_0), pressure coefficients ($d\omega/dP$), and mode Grüneisen parameters of $TbVO_4$ in the zircon phase. To obtain the mode Grüneisen parameter, $\gamma = (B_0/\omega_0)\times d\omega/dP$, the bulk modulus $B_0 = 122$ GPa is taken from Ref. [14]. Results are also compared with literature data.

Raman Mode Symmetry	ω_0[a] [cm^{-1}]	$d\omega/dP$[a] [cm^{-1}/GPa]	γ[a]	ω_0[b] [cm^{-1}]	$d\omega/dP$[b] [cm^{-1}/GPa]	ω_0[c] [cm^{-1}]	ω_0[d] [cm^{-1}]	$d\omega/dP$[d] [cm^{-1}/GPa]
$T(E_g)$	-----	-----	-----	108.9	0.90	-----	-----	-----
$T(B_{1g})$	120	0.9	0.91	117.7	1.15	121	118	0.9
$T(E_g)$	154	-0.4	-0.32	151.5	-0.92	155	152	-0.4
$R(E_g)$	246	4.6	2.28	230.9	5.01	246	243	5.0
$\nu_2(B_{2g})$	260	-1.2	-0.56	255	-1.77	261	257	-1.3
$T(B_{1g})$	-----	-----	-----	246	2.67	-----	------	------
$\nu_4(E_g)$	-----	-----	-----	371.7	0.66	-----	------	------
$\nu_2(A_{1g})$	381	1.5	0.48	364.4	1.98	380	377	1.4
$\nu_4(B_{1g})$	483	2.5	0.63	464.9	2.63	484	480	2.6
$\nu_3(B_{1g})$	809	5.5	0.83	814.6	6.08	808	807	5.9
$\nu_3(E_g)$	826	5.1	0.75	822.16	5.64	824	824	5.4
$\nu_1(A_{1g})$	885	5.6	0.77	878.4	6.1	882	883	6.0

[a] Experimental data this work. [b] Theoretical calculations this work. [c] Ref. [38]. [d] Ref.[23].

Table II: *Ab initio* calculated frequencies (ω) at 9.1 GPa and experimental frequencies at 9.6 GPa and pressure coefficients of the $TbVO_4$ in the scheelite phase. Grüneisen parameters are calculated considering B_0 = 163 GPa [14]. Present results are also compared with data calculated from Ref. [23] for P = 9.6 GPa. Phonon frequencies obtained at 1.6 GPa after pressure release are also included in the right-side column.

Raman Mode Symmetry	ω^a [cm^{-1}]	$d\omega/dP^a$ [cm^{-1}/GPa]	γ^a	ω^b [cm^{-1}]	$d\omega/dP^b$ [cm^{-1}/GPa]	ω^c [cm^{-1}]	$d\omega/dP^c$ [cm^{-1}/GPa]	ω^d [cm^{-1}]
$T(E_g)$	119	0.1	0.14	118.5	0.34			107
$T(B_g)$	140	-0.1	-0.11	140.1	-0.24	136	0.07	132
$T(B_g)$	195	2.5	2.09	192.3	1.61	194	1.9	175
$T(E_g)$	211	2.6	2.01	208.7	2.07	210	2.1	190
$\nu_2(A_g)$	246	1.2	0.80	243.6	0.60	246	0.9	236
$R(E_g)$	333	3.0	1.47	325.9	1.98	333	2.5	309
$R(A_g)$	374	3.5	1.53	354.5	2.51	373	2.7	346
$\nu_2(B_g)$	389	2.6	1.09	377.5	1.64	389	2.3	368
$\nu_4(B_g)$	434	3.2	1.20	420.5	3.03	435	2.7	408
$\nu_4(E_g)$	459	3.5	1.24	439.5	3.07	463	3.2	431
$\nu_3(E_g)$	779	4.2	0.88	779.6	3.41	777	3.7	745
$\nu_3(B_g)$	831	3.5	0.69	822.8	2.88	831	3.0	803
$\nu_1(A_g)$	861	3.7	0.70	846.3	2.74	861	3.4	831

[a] Experimental data this work, [b] Theoretical calculations this work, [c] Data obtained from Ref. [23]. [d] Data from this work obtained after pressure release at 1.6 GPa.

Table III: Experimental frequencies at 31.4 GPa and *ab initio* calculated frequencies at 31.6 GPa and pressure coefficients of the $TbVO_4$ in the fergusonite phase.

Raman Mode Symmetry	ω^a [cm^{-1}]	$d\omega/dP^a$ [cm^{-1}/GPa]	ω^b [cm^{-1}]	$d\omega/dP^b$ [cm^{-1}/GPa]
B_g	91	0.3	122.5	0.04
B_g	121	0.5	127.1	0.38
A_g	140	0.4	132.8	-0.58
A_g	213	0.6	219.3	0.86
B_g	248	0.1	236.3	0.44
A_g	278	1.2	259.7	1.08
B_g	307	0.4	271.7	3.32
B_g	362	0.3	362.8	1.08
B_g	388	1.6	387.5	2.82
A_g	416	0.5	409.3	2.28
A_g	436	0.8	414.3	1.59
A_g	508	1.2	500.7	3.38
B_g	534	0.9	502.0	2.37
B_g	570	2.0	519.5	3.92
B_g	783	1.7	827.3	1.41
A_g	836	0.8	850.3	0.85
B_g	848	2.6	855.7	3.65
A_g	922	2.1	919.5	3.27

[a] Experimental data this work, [b] Theoretical calculations this work.

TABLE IV: Calculated structural parameters for different structures.

Zircon at ambient pressure: $a = b = 7.23556$ Å and $c = 6.34152$ Å.

	Site	x	y	z
Tb	4a	0	0.75	0.125
V	4b	0	0.25	0.375
O	16h	0	0.43368	0.20072

Scheelite at 9.1 GPa: $a = b = 5.00340$ Å and $c = 11.10490$ Å.

	Site	x	y	z
Tb	4b	0	0.25	0.625
V	4a	0	0.25	0.125
O	16f	0.25418	0.10211	0.04288

Fergusonite (*C2/c*) at 26.7 GPa: $a = 6.89574$ Å , $b = 10.72828$ Å, $c = 4.89235$ Å , and $\beta = 134.983^{o}$.

	Site	x	y	z
Tb	4e	0	0.87511	0.25
V	4e	0	0.37423	0.25
O_1	8f	0.25132	0.46025	0.34540
O_2	8f	0.15745	0.28953	0.65906

Cmca at 35.4 GPa: $a = 7.30480$ Å, $b = 12.12854$ Å, and $c = 4.89861$ Å.

	Site	x	y	z
Tb	8e	0.25	0.84115	0.25
V	8f	0.5	0.58939	0.28068
O_1	8f	0.5	0.41326	0.07580
O_2	8d	0.15369	0	0.5
O_3	8f	0.5	0.79106	0.99398
O_4	8e	0.25	0.15306	0.25

Table V: Calculated Raman phonons for the Cmca structure at 35.8 GPa and pressure coefficients.

Raman Mode Symmetry	ω [cm^{-1}]	dω/dP [cm^{-1}/GPa]	Raman Mode Symmetry	ω [cm^{-1}]	dω/dP [cm^{-1}/GPa]
B_{1g}	75.4	1.64	A_g	446.4	0.45
B_{3g}	116.4	1.89	B_{3g}	459.1	0.98
A_g	161.3	1.36	B_{3g}	492.4	2.07
B_1g	165.5	0.65	B_{1g}	525.6	1.65
B_{2g}	167.0	0.87	A_g	536.4	0.95
B_{3g}	193.5	1.89	A_g	574.6	3.09
B_{3g}	211.4	1.30	B_{2g}	578.5	2.60
B_{1g}	231.2	0.06	B_{3g}	596.9	1.46
A_g	263.1	2.57	B_{2g}	625.7	2.57
B_{1g}	305.3	1.44	B_{1g}	666.0	3.20
A_g	347.1	1.13	B_{3g}	712.4	2.26
B_{3g}	360.1	2.28	A_g	720.3	-1.29
B_{2g}	373.8	2.72	A_g	720.4	1.25
B_{2g}	375.9	2.10	B_{2g}	748.2	4.27
B_{1g}	392.5	3.13	B_{1g}	784.1	3.89
B_{2g}	432.6	1.91	B_{3g}	784.4	1.30
B_{3g}	436.7	2.55	B_{3g}	800.2	1.60
B_{1g}	448.1	3.30	A_g	806.9	2.00

Figure Captions

Figure 1: (a) Raman spectra measured from $TbVO_4$ in the zircon phase between 1 atm and 6.7 GPa. (b) Experimental pressure dependence of the Raman-mode frequencies in zircon-type $TbVO_4$. The solid lines are the calculated modes. The dashed lines represent Raman modes not observed in the experiments

Figure 2: (a) Raman spectra of the scheelite phase of $TbVO_4$ at pressures between 8.3 GPa and 26.3 GPa. (b) Experimental pressure dependence of the Raman-mode frequencies in scheelite phase of $TbVO_4$. The solid lines are the calculated modes.

Figure 3: Raman spectra of $TbVO_4$ at selected pressures illustrating the post-scheelite transitions. A Raman spectrum collected after pressure release (r) is shown in the upper trace. Ticks indicate the positions for the calculated Raman modes of the fergusonite phase at 31.6 GPa and of the Cmca phase at 35.8 GPa. (b) Experimental pressure dependence of the Raman-mode frequencies in fergusonite phase of $TbVO_4$. The solid lines are the calculated modes.

Figure 4: (color online) Energy-volume curves calculated for $TbVO_4$. Since the total-energy curves of scheelite and fergusonite structures overlap, we remark the stability range of scheelite phase (fergusonite phase) using a solid (dashed) line. The inset shows differences in free energy with respect to the zircon phase.

Figure 5: Pressure evolution of the β angle of the fergusonite structure (*I2/a* setting).

Figure 6: (color online) Total and partial phonon density of states.

Figure 7: Calculated frequency of the B_{1u} silent mode of the zircon-type structure as a function of pressure.

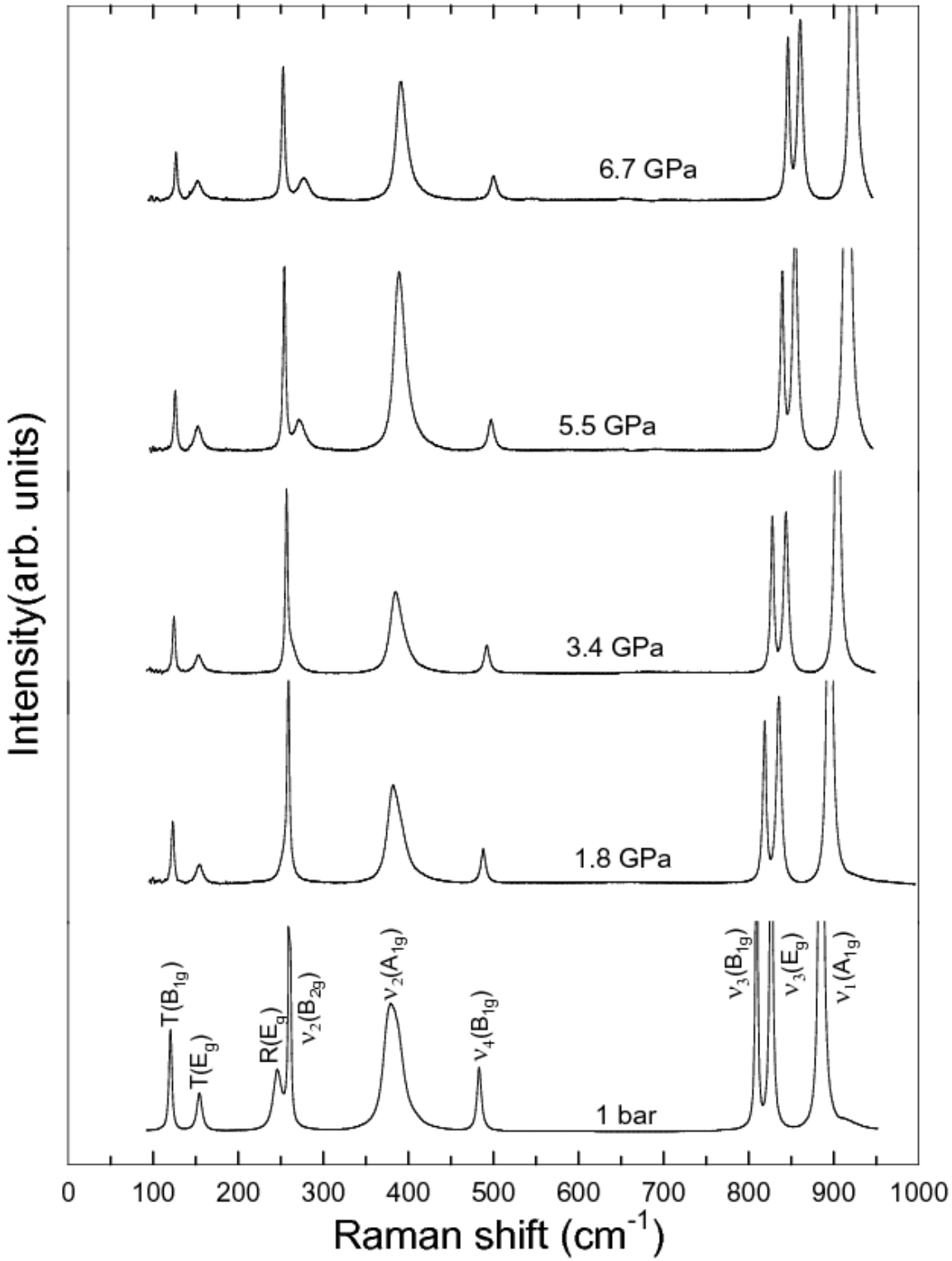
6.7 GPa
5.5 GPa
3.4 GPa
1.8 GPa
1 bar
T(B1g)
T(Eg)
R(Eg)
ν2(B2g)
ν2(A1g)
ν4(B1g)
ν3(B1g)
ν3(Eg)
ν1(A1g)
Intensity(arb. units)
0
100
200
300
400
500
600
700
800
900
1000
Raman shift (cm-1)

Figure 1(a)

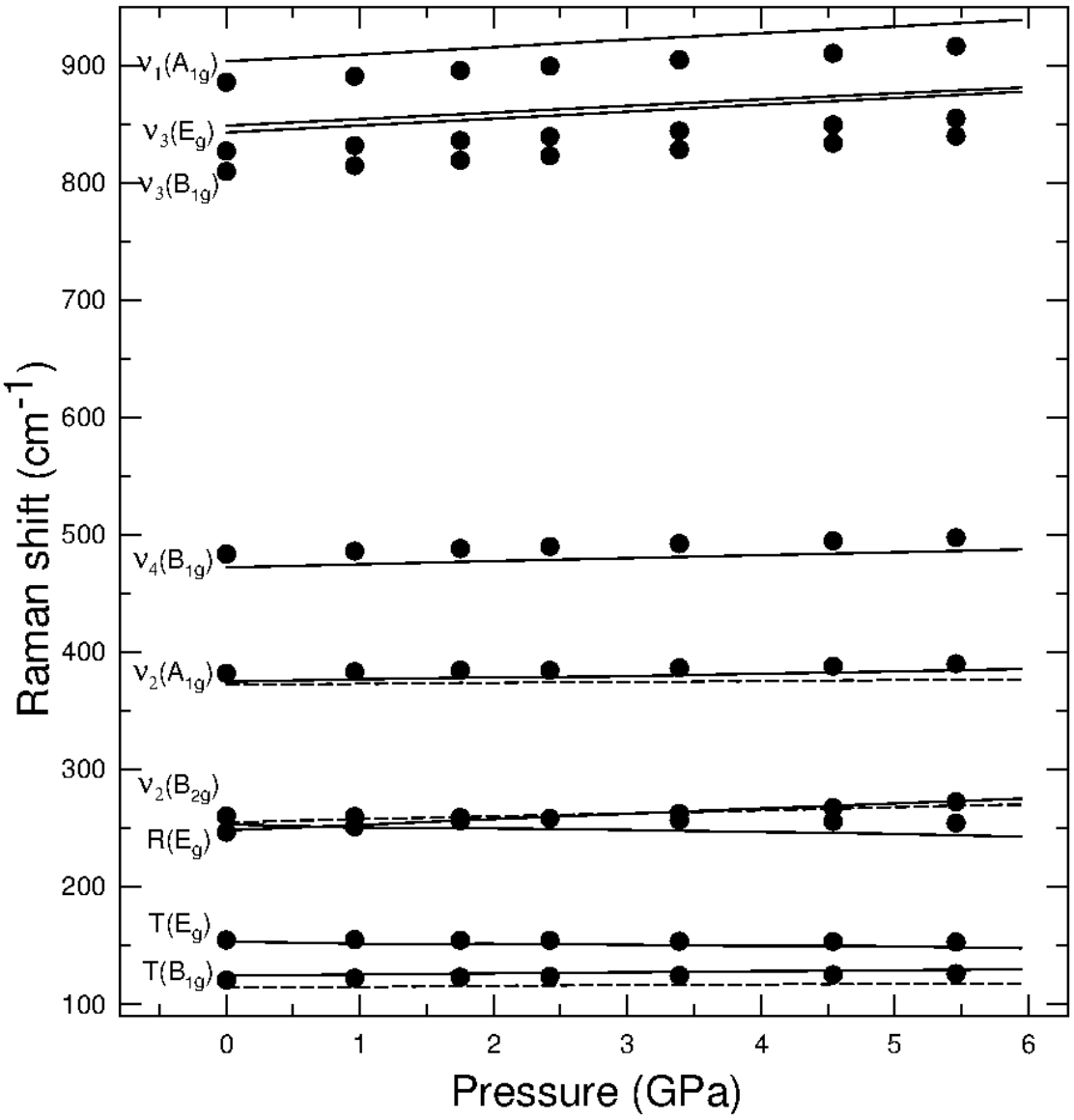
Raman shift (cm^{-1})
Pressure (GPa)
$\nu_1(A_{1g})$
$\nu_3(E_g)$
$\nu_3(B_{1g})$
$\nu_4(B_{1g})$
$\nu_2(A_{1g})$
$\nu_2(B_{2g})$
$R(E_g)$
$T(E_g)$
$T(B_{1g})$
100
200
300
400
500
600
700
800
900
0
1
2
3
4
5
6

Figure 1(b)

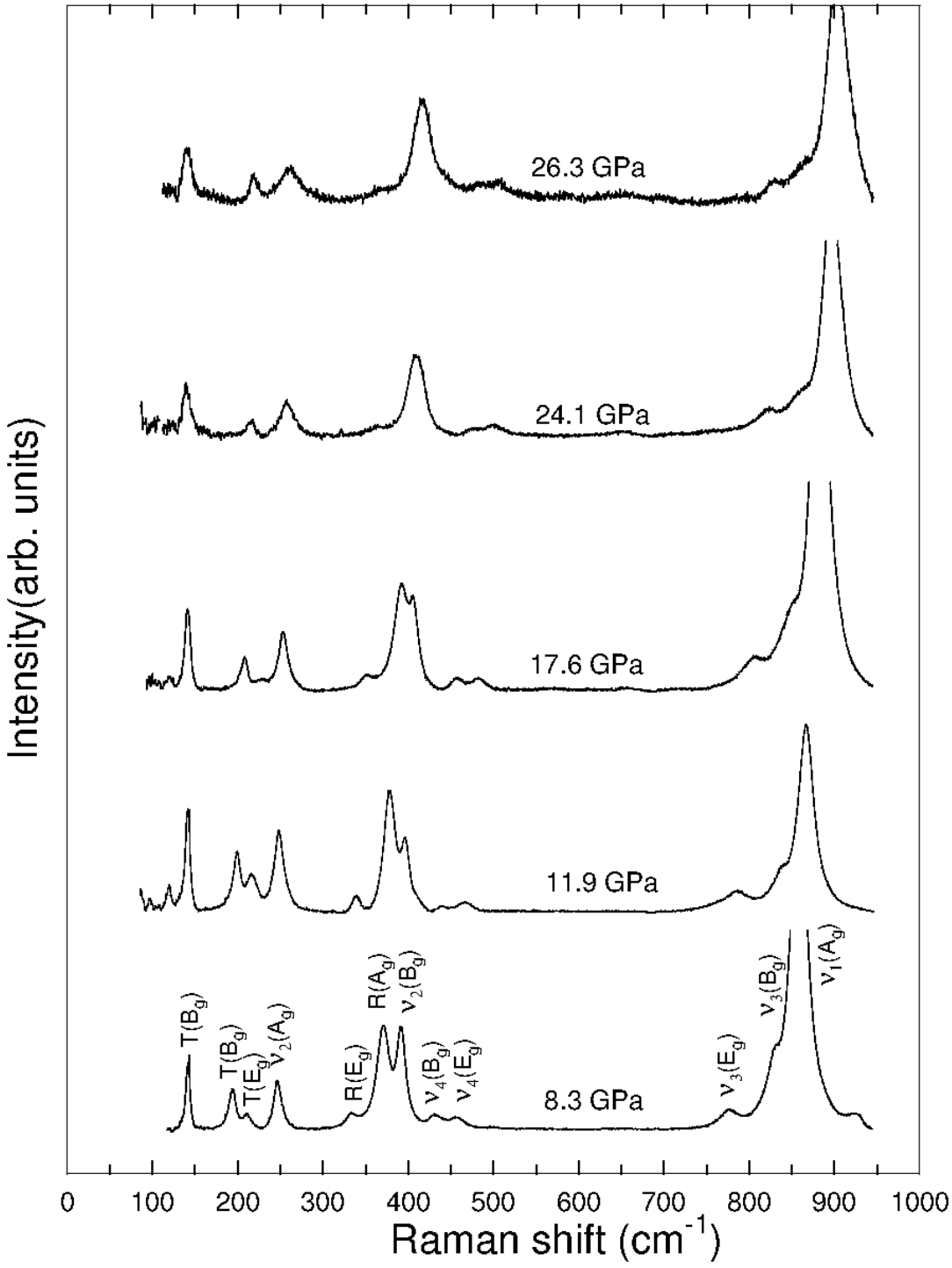
26.3 GPa
24.1 GPa
17.6 GPa
11.9 GPa
8.3 GPa
T(B$_g$)
T(B$_g$)
T(E$_g$)
ν$_2$(A$_g$)
R(E$_g$)
R(A$_g$)
ν$_2$(B$_g$)
ν$_4$(B$_g$)
ν$_4$(E$_g$)
ν$_3$(E$_g$)
ν$_3$(B$_g$)
ν$_1$(A$_g$)
Intensity(arb. units)
0
100
200
300
400
500
600
700
800
900
1000
Raman shift (cm^{-1})

Figure 2(a)

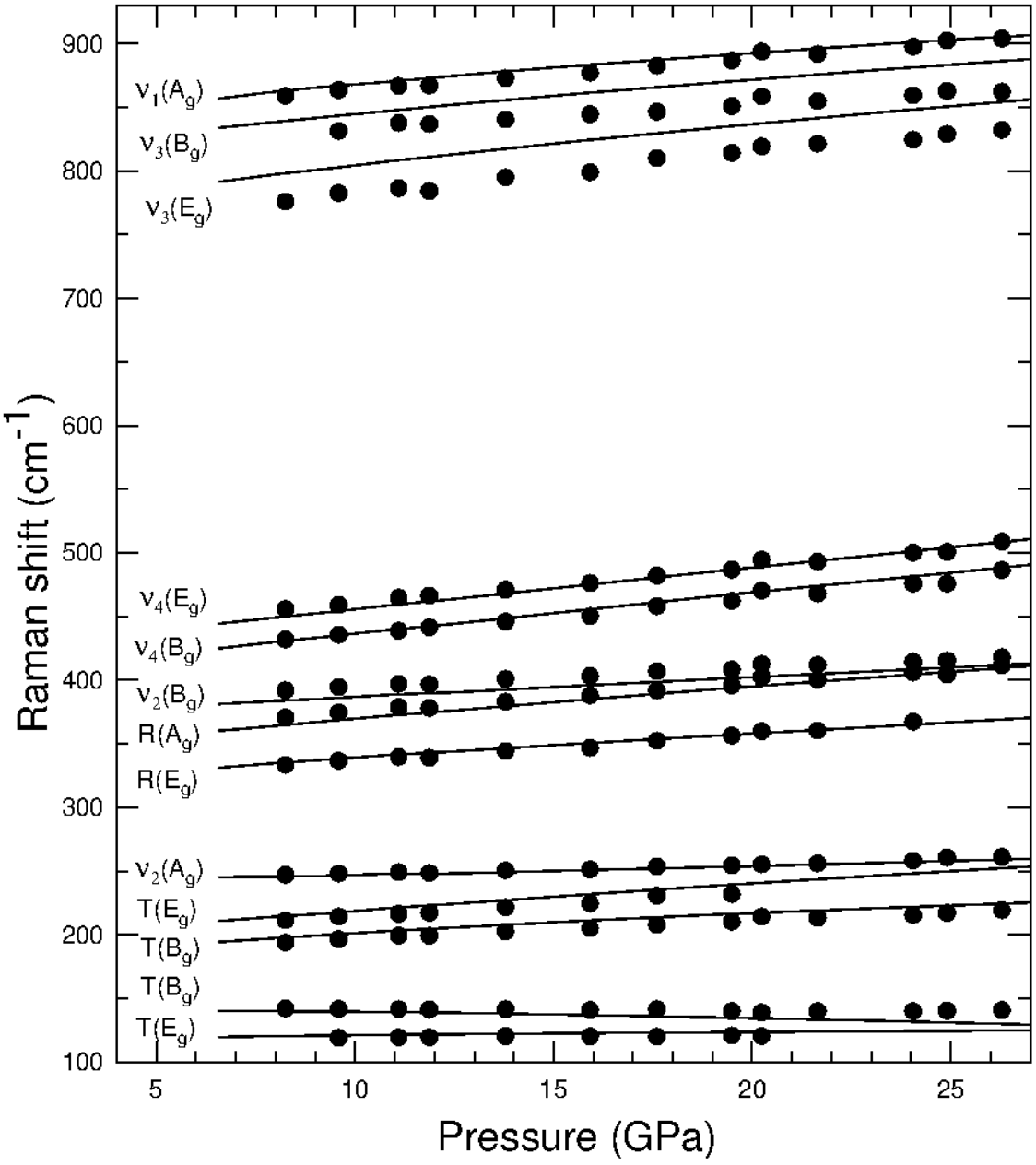
Raman shift (cm^{-1})
Pressure (GPa)
$\nu_1(A_g)$
$\nu_3(B_g)$
$\nu_3(E_g)$
$\nu_4(E_g)$
$\nu_4(B_g)$
$\nu_2(B_g)$
R(A_g)
R(E_g)
$\nu_2(A_g)$
T(E_g)
T(B_g)
T(B_g)
T(E_g)
900
800
700
600
500
400
300
200
100
5
10
15
20
25

Figure 2(b)

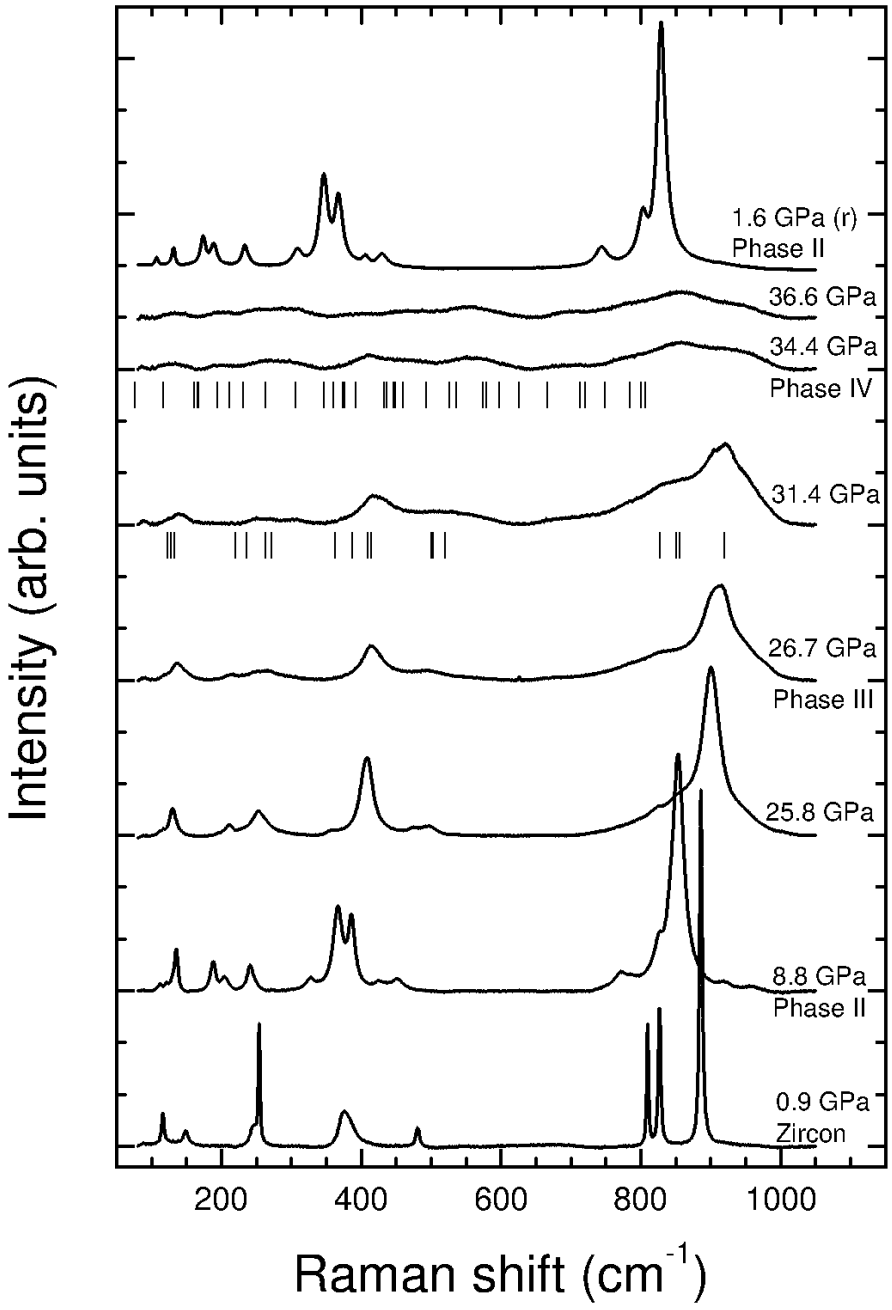
Intensity (arb. units)
1.6 GPa (r)
Phase II
36.6 GPa
34.4 GPa
Phase IV
31.4 GPa
26.7 GPa
Phase III
25.8 GPa
8.8 GPa
Phase II
0.9 GPa
Zircon
200
400
600
800
1000
Raman shift (cm-1)

Figure 3(a)

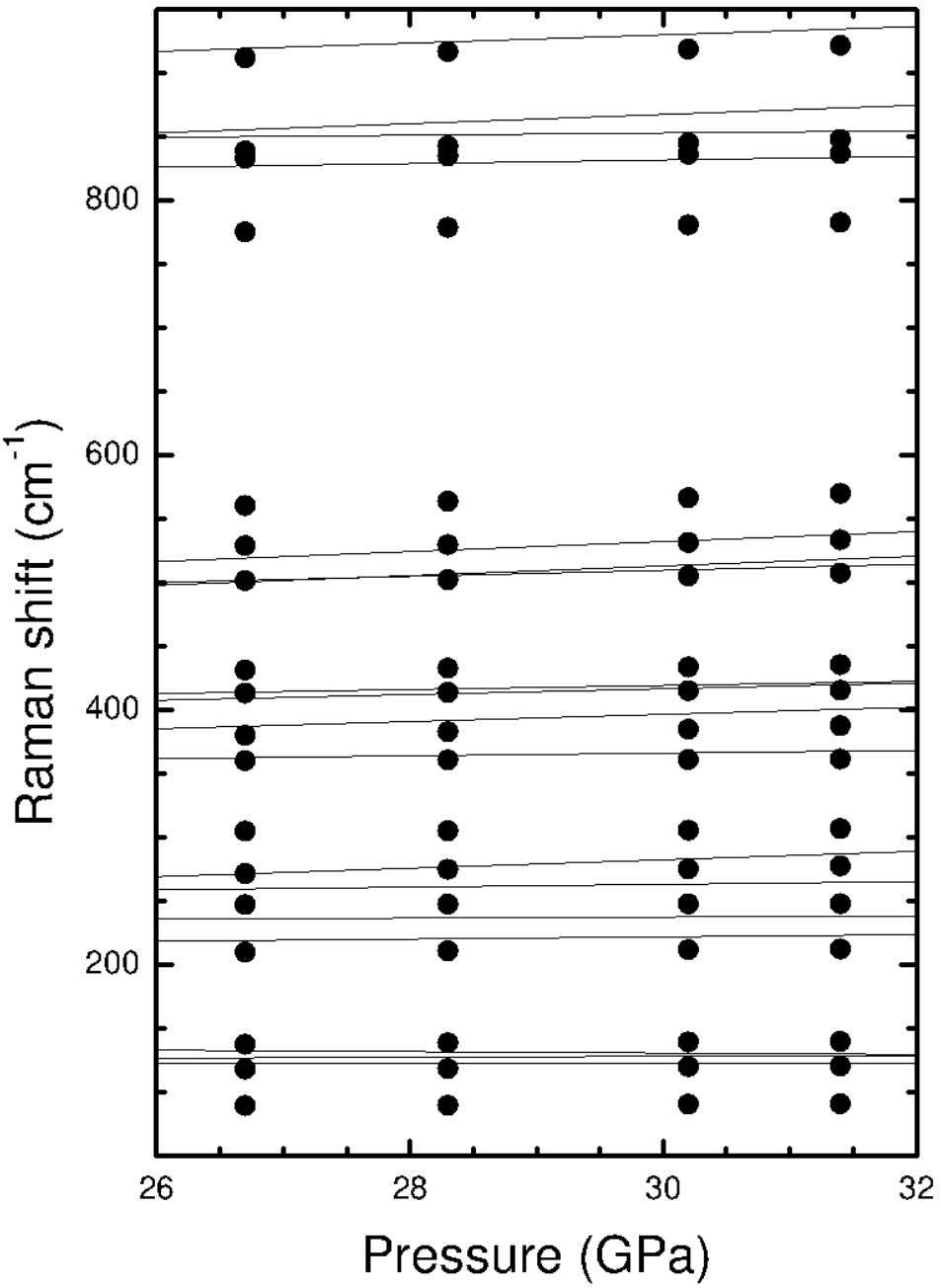

Figure 3(b)

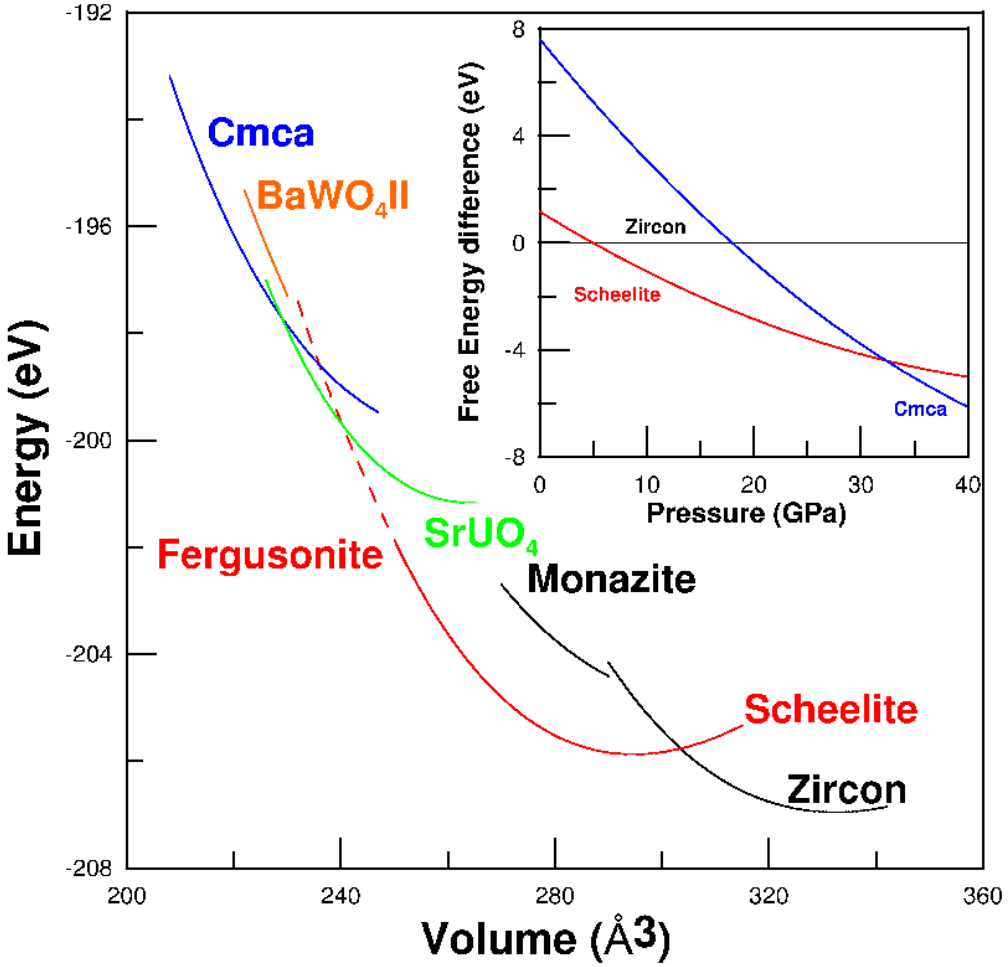
-192
-196
-200
-204
-208
Energy (eV)
200
240
280
320
360
Volume (Å3)
Cmca
BaWO4II
SrUO4
Fergusonite
Monazite
Scheelite
Zircon
8
4
0
-4
-8
Free Energy difference (eV)
Zircon
Scheelite
Cmca
0
10
20
30
40
Pressure (GPa)

Figure 4

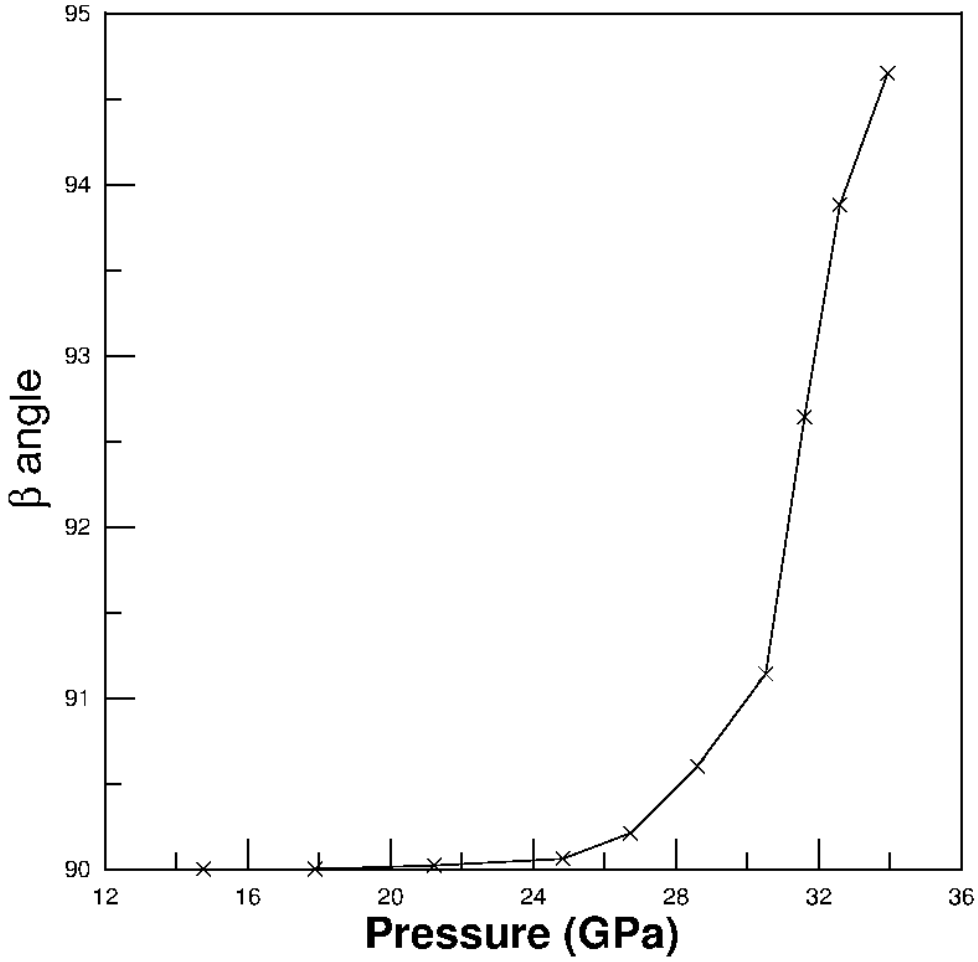

Figure 5

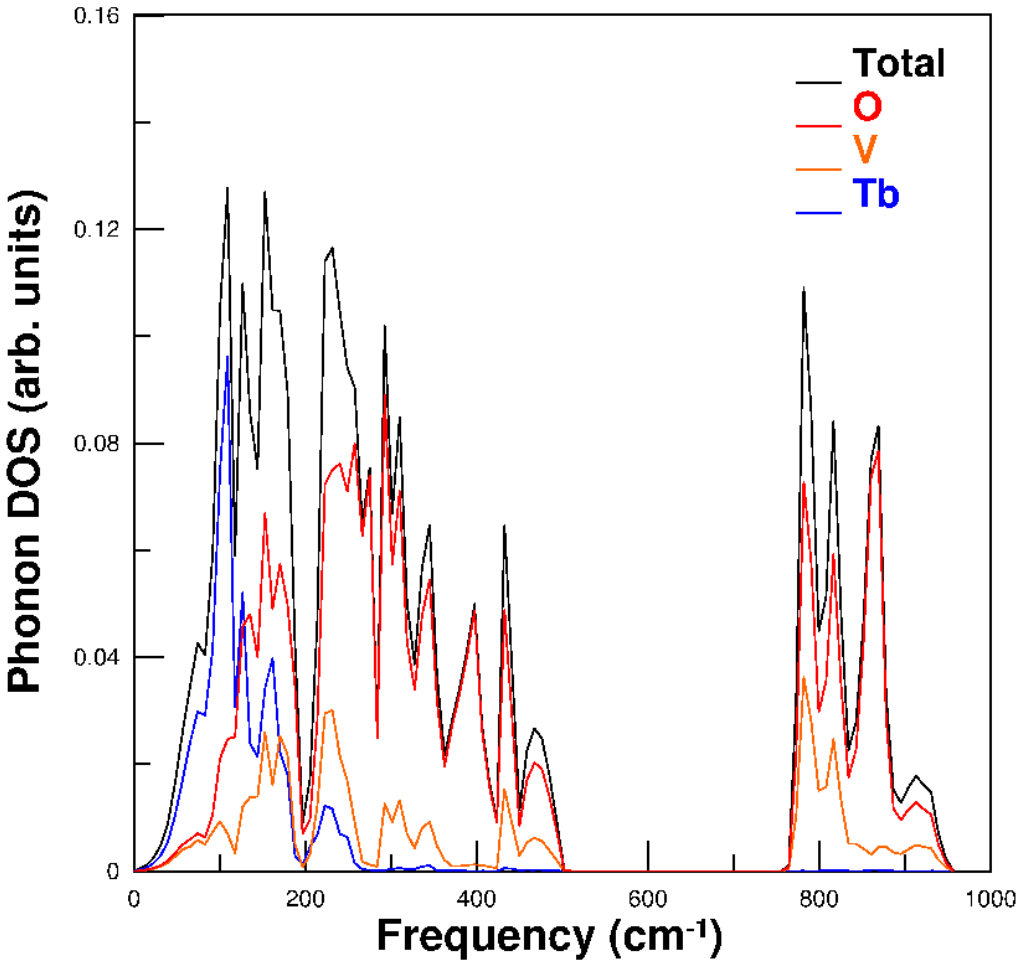
Total
O
V
Tb
Phonon DOS (arb. units)
0.16
0.12
0.08
0.04
0
0
200
400
600
800
1000
Frequency (cm-1)

Figure 6

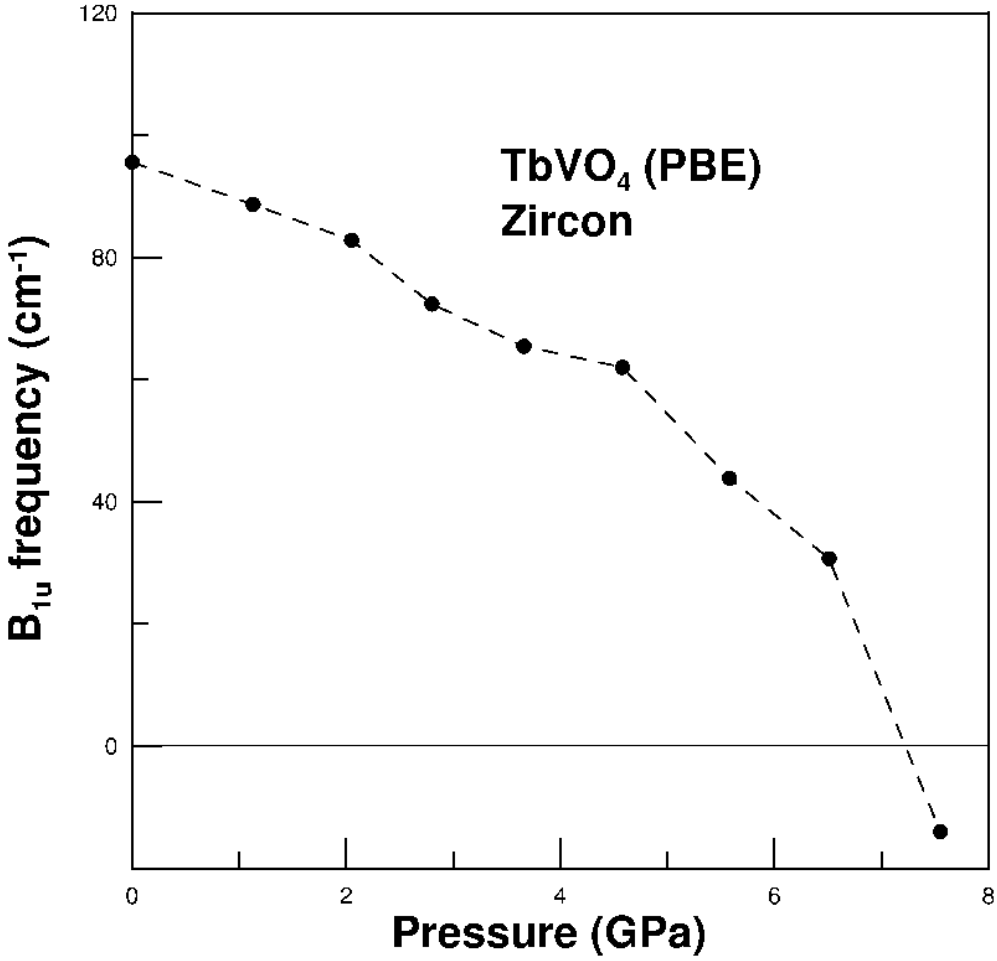
120
80
40
0
0
2
4
6
8
TbVO4 (PBE)
Zircon
B1u frequency (cm-1)
Pressure (GPa)

Figure 7